Desalination and Water Treatment
www.deswater.com

doi: 10.5004/dwt.2022.28007

248 (2022) 124–133
February

Catalytic chemical reduction of Cr(VI) from contaminated waters by the production of hydrogen radical on the cellulose sulfate microfibers coated with palladium nanocatalyst

Mitra Jokar[a], Gholamreza Nabi Bidhendi[b,*], Hossein Naeimi[a]

[a]*Department of Organic Chemistry, Faculty of Chemistry, University of Kashan, Kashan, Iran, emails: mitrajokar596@yahoo.com (M. Jokar), naeimi@kashanu.ac.ir (H. Naeimi)*
[b]*School of Environment, College of Engineering, University of Tehran, Tehran, Iran, email: ghhendi@ut.ac.ir*

Received 7 May 2021; Accepted 9 November 2021

ABSTRACT

In this study, the removal of Cr(VI) from contaminated waters was studied via a chemical reduction of Cr(VI) on cellulose sulfate microfibers coated with palladium nanocatalyst. In this catalytic procedure, hydrogen gas was generated utilizing an electrochemical cell containing graphite electrodes. Characterization of the prepared catalyst was done using scanning electron microscopy, energy-dispersive X-ray analysis, Fourier-transformed infrared spectroscopy, and thermalgravimetric analyses. The Box–Behnken model of response surface methodology was used to optimize the adsorption process. The effects of main variables including current density, initial concentration of Cr(VI), and time and their interactions on the removal efficiency of Cr(VI) were assessed. Under the optimal conditions (0.1 A and 15 min), the removal efficiency of 98% was achieved for Cr(VI). The examination of recovery indicated that the performance of the prepared catalyst decreased about 10% after 10 cycles of usage.

Keywords: Catalytic reduction; Chromium (VI); Palladium; Cellulose sulfate; Water

1. Introduction

Heavy metals are one of the most important environmental pollutants with harmful and carcinogenic effects. The presence of heavy metals in drinking water, even at low concentrations, is a major concern for human health due to their high toxicity [1]. The accumulation of these metals at low concentrations in the human body causes disease. Chromium is one of the most famous and widely used heavy metals, which is found in various oxidation states, hexavalent (Cr(VI)) and trivalent (Cr(III)) in the environment. It was found that Cr(VI) is 500 times more toxic than Cr(III) [2,3]. The International Agency for Research on Cancer has classified Cr(VI) as a class I carcinogen due to its high toxicity, mutagenicity, and carcinogenicity [4]. The world health organization (WHO) stipulates that the maximum Cr(VI) concentration of 0.1 and 0.05 mg L^{-1} for treated wastewater and drinking water, respectively [5]. The wastewater of industrial activities such as leather tanning, steel and alloys manufacturing, electroplating, petroleum refining, wood preservation, and the production of pulp, paper, and pigments are the main sources of contaminants affecting the environment [6–9]. Unlike Cr(VI), which is highly toxic, soluble, and mobile, Cr(III) ions have low toxicity and mobility and are susceptible to precipitate or adsorb on various adsorbents [10]. Cr(III) is needed in small quantities for humans and animals as an important nutrient used for the metabolism of sugars, proteins, and

* Corresponding author.

fat [11]. Therefore, to increase the elimination performance of total chromium in the treatment process of contaminated waters, conversion of Cr(VI) to Cr(III) has an essential role.

Nowadays, to reduce Cr(VI) to Cr(III), several cheaper and practical technologies including physicochemical methods [12,13], electrochemical techniques including electrocoagulation using different electrodes [14,15], photocatalytic degradation [16,17], and biological methods [18] have been established. Removal of Cr(VI) based on the chemical transformation of Cr(VI) to Cr(III), has been done on the interfacial surface of commercial adsorbents such as activated carbon, Fe(0), and biochar [19]. In this strategy, reducing reagents, such as L-ascorbic acid [20,21], Fe(II) [22], and sodium borohydride ($NaBH_4$) [23] were used. However, releasing new contaminants into the water source is a serious consequence of the removal of Cr(VI) under reduction conditions [24]. In contrast, no residual contamination, no chemical requirement, and ease of operation are the advantages of the electrochemical method [25,26]. This method suffers from some limitations such as low removal efficiency and intensive energy requirements [27]. In order to effectively eliminate Cr(VI) with a significant reaction rate, catalytic hydrogenation of Cr(VI) by palladium nanocatalyst was utilized. However, the application and development of this method is limited due to the potential safety problem concerning H_2 handling [28]. To overcome the mentioned issues, electrochemical method has been integrated with catalytic reduction process. For this purpose, Pd catalyst was immobilized on the surface of cathode and electrochemical reduction reaction was done on the electrodes.

The typical process for the treatment of hexavalent chromium-contaminated waters is the electrochemical reduction of Cr(VI) to Cr(III) followed by a simple process such as adsorption. Activated carbon, clays, modified plant wastes, and chitin are common substances used as effective adsorbents in the adsorption process. Due to the porosity and high surface area of cellulose, it is a suitable material to use as an adsorbent. Additionally, it is biodegradable, renewable, and inexpensive. Nevertheless, due to the lack of proper functional groups, cellulose is not able to eliminate pollutants and its surface modification through its hydroxyl groups is necessary to convert it to a suitable adsorbent [29–33].

In this study, Pd NPs were immobilized on the surface of synthesized cellulose sulfate from the natural cotton and used for electrochemical removal of Cr(VI) from contaminated water. Fourier-transformed infrared spectroscopy (FTIR), scanning electron microscopy (SEM), energy-dispersive X-ray analysis (EDX), and thermalgravimetric analysis (TGA) techniques were used for the characterization of the prepared modified cellulose microfibers. All of the factors involved in the removal process of the Cr(VI), such as current density, initial concentration of Cr(VI), and reaction time were investigated and optimized.

2. Experimental

2.1. Materials

All chemicals and reagents used in this research including, chlorosulfonic acid, N,N-dimethylformamide, $PdCl_2$, H_2SO_4, $NaBH_4$, Na_2CO_3, and $K_2Cr_2O_7$ were obtained from Merck (Darmstadt, Germany) or Sigma-Aldrich (St. Louis, MO, USA) and used without further purification. Sodium chloride (NaCl), potassium chloride (KCl), magnesium chloride ($MgCl_2$), potassium nitrate (KNO_3), sodium sulfate (Na_2SO_4), magnesium sulfate ($MgSO_4$), and calcium sulfate ($CaSO_4$) were used to investigate the effect of co-existing ions. Natural cotton, as a source of cellulose microfibers, was obtained from a local market in Kashan, Iran. Before modification of the cotton surface, it was dried at 50°C overnight. Deionized water purified via a Milli-Q purification system (Millipore, Bedford, MA) was used in all experimental tests.

2.2. Preparation of fibrous cellulose sulfate

Sulfonation of natural cotton fiber was conducted using CSA, resulting in cellulose sulfate as anionic biomass. [34]. In a typical procedure, a proper amount of pre-dried cotton microfiber (20 g) was immersed in 100 mL of DMF and soaked for 15 min at 4°C. Afterward, 50 g of CSA was added dropwise to 150 mL of DMF in an ice bath. At that point, the resultant solution was gently added to the cotton microfiber soaked in DMF and shacked in an ice bath for 3 h. Then, the functionalized cotton microfibers were separated from the reaction mixture using vacuum filtration through a 1 μm membrane filter. Subsequently, the obtained functionalized cotton microfiber was neutralized with 5% (w/v) sodium bicarbonate solution and washed three times with deionized water. Lastly, modified cellulose sulfate was filtered and washed with deionized water several times.

2.3. Preparation of the catalyst

To immobilize Pd NPs on the surface of cellulose sulfate fibers, 5 g of cellulose sulfate sodium salt was immersed in 50 mL of an aqueous solution of H_2SO_4 (1 M) for 10 min at 60°C. Then 0.05 g of $PdCl_2$, which was dissolved in few drops of concentrated hydrochloric acid, was added to the cellulose sulfate mixture while shaking for 15 min. Then, the resulting mixture was reduced with a cold aqueous solution of $NaBH_4$ for 30 min to form Pd nanoparticles on the surface of the cellulose sulfate [27]. The prepared Pd NP-containing fibrous catalyst was rinsed thoroughly with water, dried under vacuum at room temperature, and stored for future use.

2.4. Catalyst characterization

Fourier-transformed infrared (FTIR) spectra of the natural cotton, cellulose sulfate, and Pd NP-containing cellulose sulfate were recorded by means of a Burker FTIR spectrometer at a wavenumber range of 4,000–400 cm^{-1} under ambient conditions. For X-ray diffraction analysis, an X-ray diffractometer (XRD, PAN, analytical B.V. – X'Pert PRO MPD) equipped with Cu Kα radiation at 2θ of 10°–90° was used. The microstructure and morphology of as-prepared the catalyst before and after immobilization of Pd NPs were investigated using scanning electron microscopy (SEM, JSM-5600LV, JEOL Ltd., Japan) with an operating voltage of 15 kV. Energy-dispersive X-ray analysis (EDS, IE300X, Oxford, U.K.) was used to analyze the elemental

composition of the catalyst. Thermal gravimetric analysis was done using a thermogravimetric analyzer (TGA, Bähr STA 503 instrument, GmbH, Germany) with a heating rate of 10°C/min in an air atmosphere. All UV-Vis absorption measurements were done on a UV-Vis spectrophotometer (Hatch, DR5000, USA).

2.5. Electrochemical cell

An electrochemical cell made of Plexiglas with a dimension of (5 cm × 5 cm × 10 cm) equipped with graphite electrodes (8 cm × 5 cm × 0.5 cm) was used to generate hydrogen gas during the catalytic reduction process of chromium (IV). An appropriate amount of the prepared catalyst was packed between the two electrodes. The useful volume of the electrochemical cell to evaluate all variables was 100 mL. In all experiments, the current density was adjusted using an HY3020D DC power supply (0–30 V, and 0–20 Å) and the solution was stirred with a magnetic stirrer during the process.

2.6. Typical procedure to catalytic removal of Cr(VI)

The catalytic removal process was done using the electrochemical cell in the batch method. A stock solution (1,000 mg mL^{-1}) of Cr(VI) was used to prepare different concentrations of Cr(VI) solution in deionized water. In all experimental tests, 100 mL of an aqueous solution of the Cr(VI) with the desired initial concentration was added to the cell and the reaction was started. At the given time of the reaction, samples were withdrawn and the remaining concentration of Cr(VI) in the solution was determined by UV-Vis spectrometer at 540 nm according to standard methods [35]. The removal efficiency of Cr(VI) was calculated as shown in the following equation [19]:

$$\mathrm{Cr(VI)\ removal\ \%} = \frac{(C_0 - C_t)}{C_0} \times 100 \quad (1)$$

where C_0 and C_t are the concentration of the Cr(VI) (mg L^{-1}) at the beginning and end of the reaction, respectively.

2.7. Design of experiments

To optimize the experimental conditions and define the importance of the independent parameters and their interaction, the Box–Behnken design (BBD) was employed. Firstly, a number of tests were done to choose the main parameters and their effective ranges. According to the obtained results, three main variables including current density (*A*), initial concentration of Cr(VI) (*B*), and time of reaction (*C*) were chosen. Three different levels (–1, 0, and +1) were set for each input variable. The levels and the ranges of these variables are shown in Table 1.

The number of whole test runs was calculated according to the following equation:

$$N = 2k(k-1) + N_o \quad (2)$$

where N_o is the number of the central points, and k is the number of independent factors. Three independent variables and five focal points were selected, so the whole number of experimental tests was 17. Additionally, to estimate the experimental error, 5 replicate tests were done in the center point. Table 2 shows the designed matrix and experimental data. To design the experiments and validate the fitted model, Design–Expert 10 (Stat-Ease Inc., USA) was used.

3. Results and discussion

3.1. Catalyst characterization

The morphology of the sulfonated cotton microfibers containing Pd NPs was investigated by SEM. As shown in Fig. 1, microfibers of sulfonated cotton are shorter than natural cotton microfibers due to the aging process in the acidic medium, which is consistent with the structure of sulfonated cotton microfibers in the literature [36]. Additionally, a large number of white Pd NPs can be obviously seen on the surface of the sulfonated cotton microfibers, which confirmed the successful formation of the Pd NPs. Also, it seems that the Pd NPs are distributed homogeneously onto the surface of cotton microfibers.

EDX analysis was used for the qualitative and quantitative analysis of elemental composition on the surface of the modified cotton microfibers as shown in Fig. 2. The existence of the Pd element shows the effective immobilization of Pd NPs on the surface of the microfibers.

The FTIR spectra of the natural cotton, cellulose sulfate, and Pd NP-containing cellulose sulfate are shown in Fig. 3, respectively. The strong absorption peak at 3,400 cm^{-1} is characteristic of the hydroxyl (OH) groups of natural cellulose. The peak observed at 2,900 cm^{-1} is related to the stretching vibration of C–H present in cellulose, and the absorption band at 1,630 cm^{-1} is related to the presence of water in the cotton microfibers. The peak at 1,428 cm^{-1} is characteristic of the CH_2 symmetric bending of the cellulose [37]. The bands observed at 1,230 and 1,180 cm^{-1} at

Table 1
Experimental ranges and three levels of the independent variables

Variables	Factor	Unit	Levels		
			–1	0	+1
Current density	*A*	A	0.010	0.055	0.100
Initial concentration of Cr(VI)	*B*	mg L^{-1}	0.5	1.75	3
Time of reaction	*C*	min	1	8	15

Table 2
RSM designed matrix, experimental, and predicted values

Run	Variables			Removal efficiency (%)	
	Current (A)	Cr(VI) (mg L^{-1})	Time (min)	Actual value	Predicted value
	A	*B*	*C*		
1	0.055	0.5	1	100	99
2	0.055	1.75	8	85.5	85.7
3	0.01	1.75	15	51	50.6
4	0.01	1.75	1	46.2	45.7
5	0.055	1.75	8	87	85.7
6	0.055	1.75	8	84.5	85.7
7	0.01	3	8	21.2	20.6
8	0.1	1.75	15	99.1	99.5
9	0.055	3	1	52.3	53.2
10	0.1	0.5	8	100	100
11	0.055	1.75	8	88.1	85.7
12	0.1	3	8	88.5	87.1
13	0.01	0.5	8	77.7	79.1
14	0.055	1.75	8	83.5	85.7
15	0.055	3	15	72	72.9
16	0.1	1.75	1	84.4	84.7
17	0.055	0.5	15	100	99

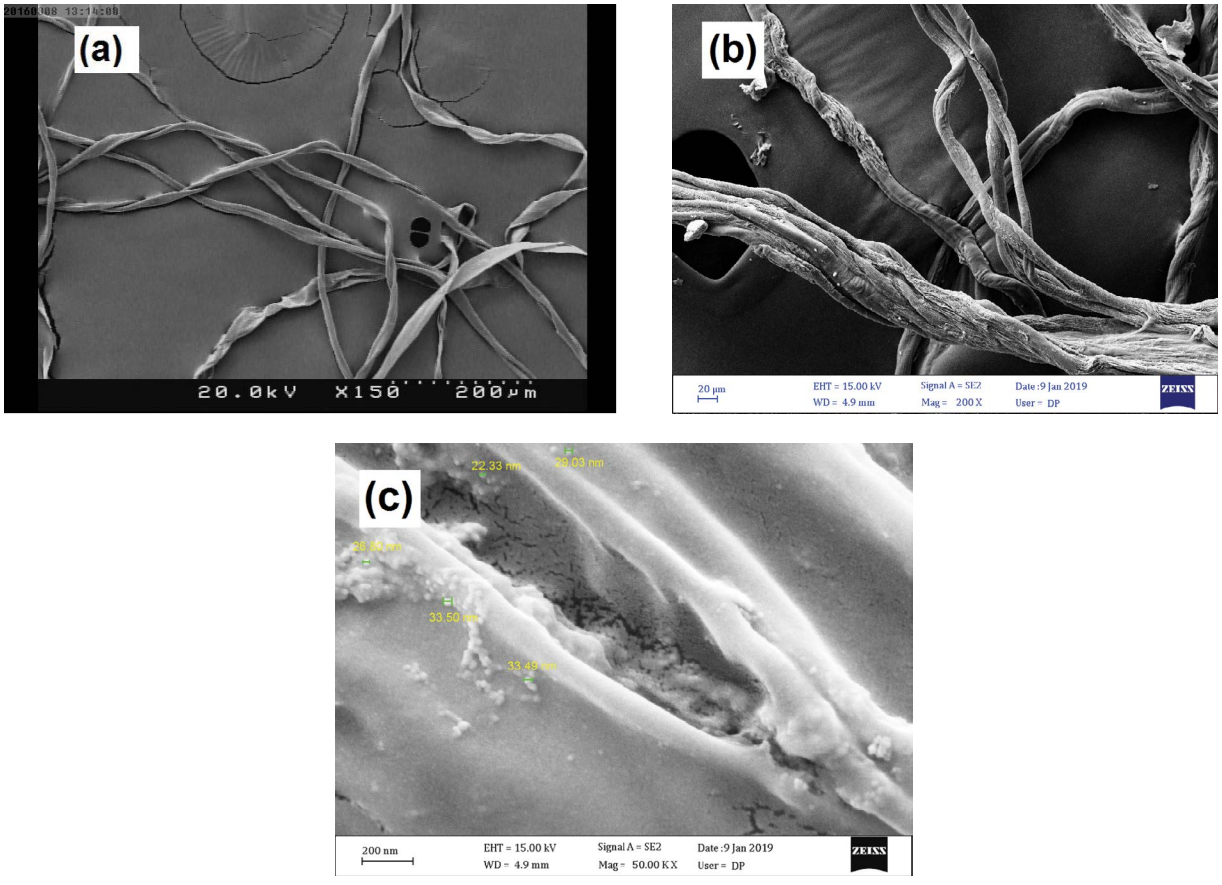

Fig. 1. SEM images of (a) cotton, 200 µm; nanocomposite (b) 20 µm and (c) 200 nm.

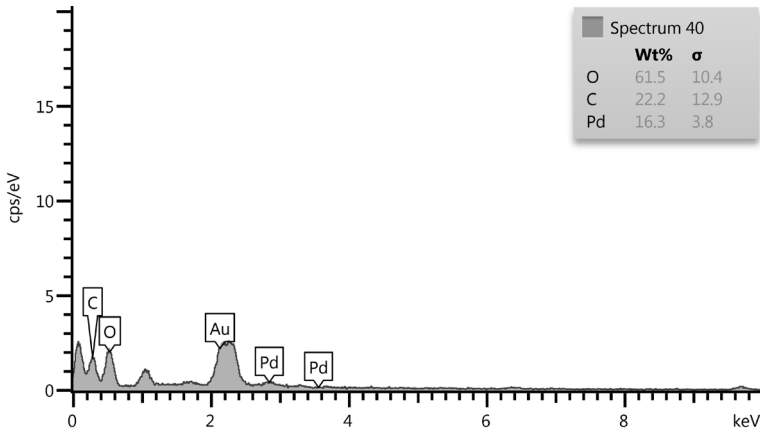

Fig. 2. EDX analysis of sulfonated cotton microfibers containing Pd NPs.

the spectrum of the cellulose sulfate and Pd NP-containing cellulose sulfate correspond to asymmetric stretching vibrations, and the bond at 610 cm^{-1} is related to the symmetric vibration of the sulfate group.

TGA graphs of the modified cellulose microfibers with and without Pd NPs are demonstrated in Fig. 4. Slight weight loss is due to water evaporation. As the temperature increased, the weight decreased sharply for both the Pd-free and Pd NP-assembled modified cellulose microfibers as a result of the decomposition of cellulose. The loading percentage of Pd NPs can be calculated by comparing the final weight of the Pd-free (a) and Pd NP-assembled (b) sulfonated cellulose microfibers.

3.2. Statistical analysis

According to the obtained quadratic model using BBD, the removal efficiency of Cr(VI) is a function of current density (A), initial concentration of Cr(VI) (B), and time of reaction (C). The double interactions are shown with AB, AC, and BC, while A^2, B^2, and C^2 are related to the quadratic effects. A confidence level of 95% was used for statistical analysis.

$$\text{Removal}\,(\%) = 85.72 + 21.99\times A - 17.96\times B + 4.90\times C + 11.25\times AB + 2.48\times AC + 4.92\times BC - 12.39\times A^2 - 1.49\times B^2 - 3.16\times C^2 \quad (3)$$

Validation of the designed model and significance of main variables was investigated using analysis of variance (ANOVA). According to the results given in Table 3, the term A with a larger F-value and the smaller p-value was the greatest important variable, while the term B^2 was the least important factor with an F-value and p-value of 2.88 and 0.1333, respectively [38].

Table 3
ANOVA results of the quadratic model

Variable	SS[a]	dF[b]	MS[c]	F-value	p-value
Model	7,999.22	9	888.80	275.96	<0.0001
A-current	3,867.60	1	3,867.60	1,200.83	<0.0001
B-Cr(IV)	2,581.21	1	2,581.21	801.42	<0.0001
C-time	192.08	1	192.08	59.64	0.0001
AB	506.25	1	506.25	157.18	<0.0001
AC	24.50	1	24.50	7.61	0.0282
BC	97.02	1	97.02	30.12	0.0009
A^2	645.85	1	645.85	200.52	<0.0001
B^2	9.29	1	9.29	2.88	0.1333
C^2	42.04	1	42.04	13.05	0.0086
Residual	22.55	7	3.22		
Lack of fit	8.78	3	2.93	0.85	0.5346
Pure error	13.77	4	3.44		
Cor. total	8,021.77	16			

[a]Sum of square.
[b]Degree of freedom.
[c]Mean square R^2 = 0.9972, Adj. R^2 = 0.9936, Pred. R^2 = 0.9798.

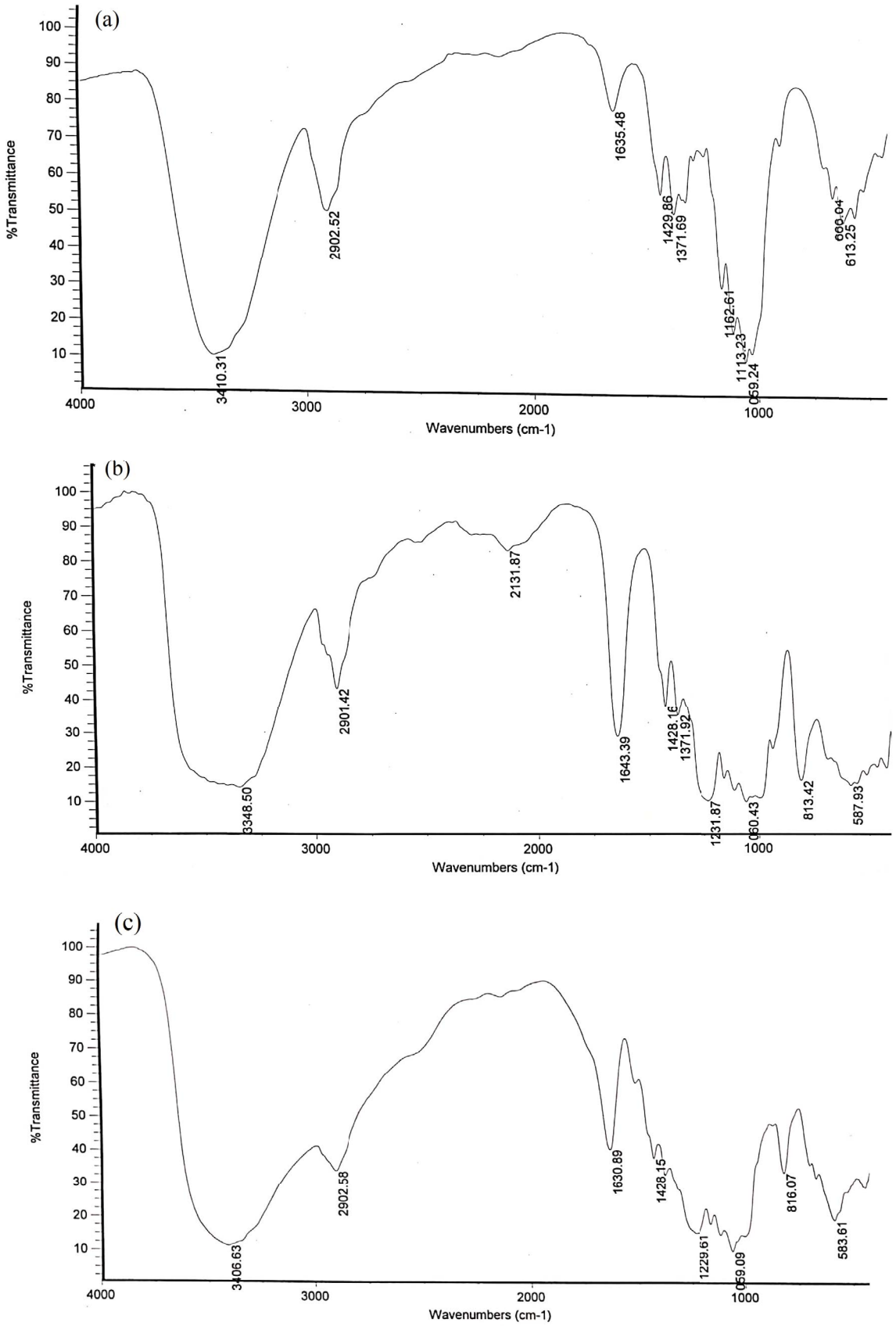

Fig. 3. FTIR spectra of the (a) natural cotton microfiber, (b) cellulose sulfate, and (c) Pd NP-containing cellulose sulfate, respectively.

As can be seen, the results indicated that the model *F*-value of response is 275.96 proving the validity of the model. Moreover, the model *p*-value of <0.0001 represents the validity of the model in the studied range of main factors.

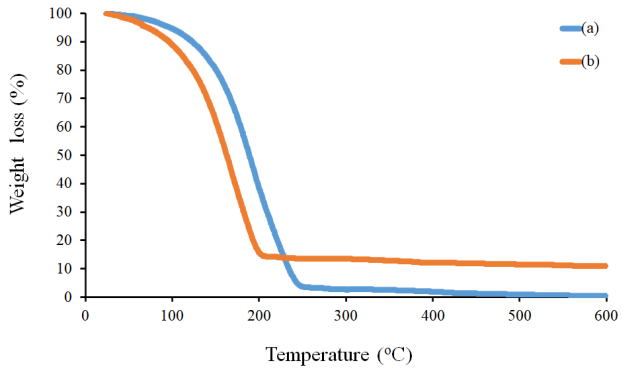

Fig. 4. TGA curves of the (a) Pd-free and (b) Pd NP-assembled cellulose sulfate.

The pure error, which was represented by the *p*-value of lack of fit, was not significant (0.5346), indicating that the model fitted well with the experimental data. Furthermore, the accuracy of the model was established by the high values of the adjusted R^2 (99.36%) and predicted R^2 (97.98%).

3.3. Impact of independent variables and interactions of them on removal efficiency of Cr(VI)

In order to compare the effect of main independent variables on the removal efficiency of Cr(VI), a perturbation plot was used. As can be seen in Fig. 5a, all parameters have a significant effect on the removal efficiency of Cr(VI). Nevertheless, the impact of time was less than that of current density and initial concentration of Cr(VI). Fig. 5b–d demonstrates the response surface plots obtained from equation (3). Fig. 5b shows the impact of current density and initial concentration of Cr(VI) at a constant time on the removal efficiency. Obviously, as the current density and/or time increased, the removal efficiency also increased. The interaction of Cr(VI) concentration with time

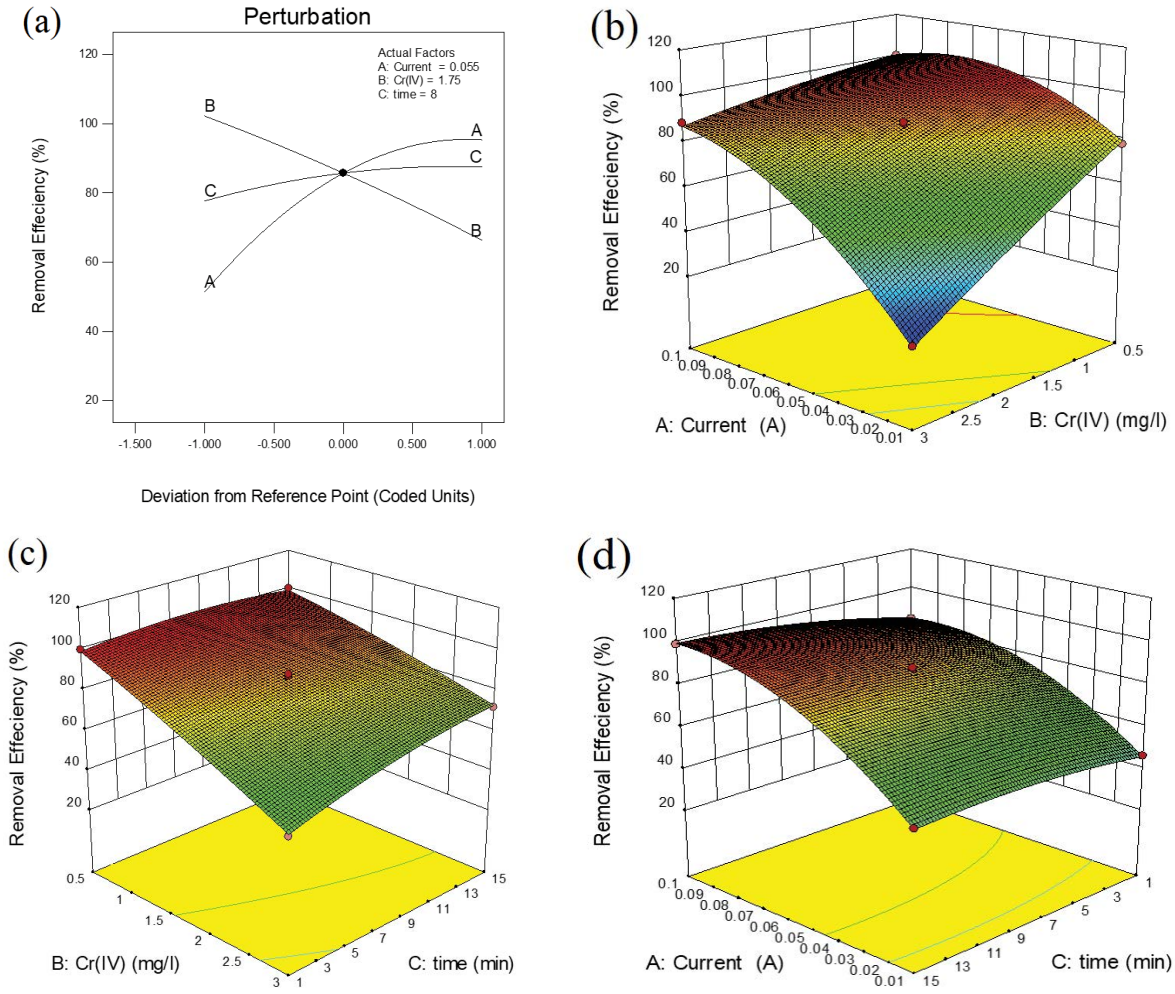

Fig. 5. (a) Perturbation plots for Cr(VI) removal, and the 3D response surface plots; (b) interactive effect of initial concentration of Cr(VI) and current density, (c) interactive effect of initial concentration of Cr(VI) and time, and (d) interactive effect of current density and time, while time, current density, and initial concentration of Cr(VI) at the level of 0, respectively.

is shown in Fig. 5c. It is obvious that by increasing the time at the low level of the initial concentration of Cr(VI), the removal efficiency of the process remained approximately constant. However, by increasing the time at the higher levels of the Cr(VI) concentration, the removal efficiency of Cr(VI) significantly increased. According to Fig. 5d, the interaction between current density and time was notable. It is clear that at low current density, more time is needed to remove Cr(VI), while by increasing current density, the time required for Cr(VI) removal is also decreased.

3.4. Mechanism of Cr(VI) reduction

Fig. 6 demonstrates the reduction-adsorption mechanism of Cr(VI) in the electroreduction cell. After the electrochemical production of the hydrogen molecules on the surface of the electrode, the produced hydrogen molecules are adsorbed on Pd NPs surface and transformed into active hydrogen radicals. After that, the bonded hydrogen radicals, as a strong reducing agent, react with Cr(VI) ions and convert them to Cr(III) ions, which are subsequently adsorbed on the surface of the modified sulfonated cotton microfibers.

3.5. Effect of co-existing ions on the removal efficiency of Cr(VI)

Effect of various co-existing ions such as Na^+, K^+, Ca^{2+}, Mg^{2+}, Cl^-, NO_3^-, SO_4^{2-}, and CO_3^{2-} on the removal efficiency of Cr(VI) was investigated in the different experiments, and the results are shown in Fig. 7. According to the results, the presence of the different ions had no destructive interference in Cr(VI) removal efficiency.

3.6. Reusability of the catalyst

Since palladium is an expensive metal, the reusability of the Pd catalyst is critical. Fig. 8 shows the catalyst performance up to 10 cycles. As can be seen, a 10% reduction in the performance of the catalyst was observed after 10 cycles, showing good reusability.

4. Conclusion

In the present study, an effective palladium catalyst coated on cellulose sulfate microfibers was fabricated by a coating of Pd NPs on the synthesized cellulose sulfate as support. Moreover, the cellulose sulfate was prepared by sulfonation of natural cotton fiber using chlorosulfonic acid. The Pd containing cellulose sulfate catalyst was characterized by FTIR, SEM, TGA, and EDX analyses. The presence of cellulose sulfate as the support of the catalyst improved the removal efficiency significantly due to its porosity and high surface area. A Box–Behnken

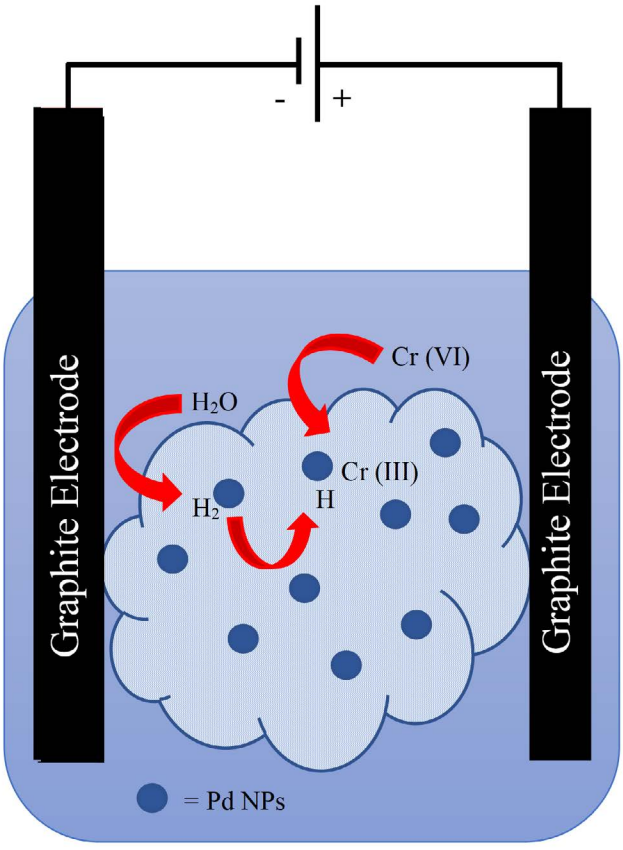

Fig. 6. The reduction–adsorption mechanism of Cr(VI) ions in the electroreduction cell.

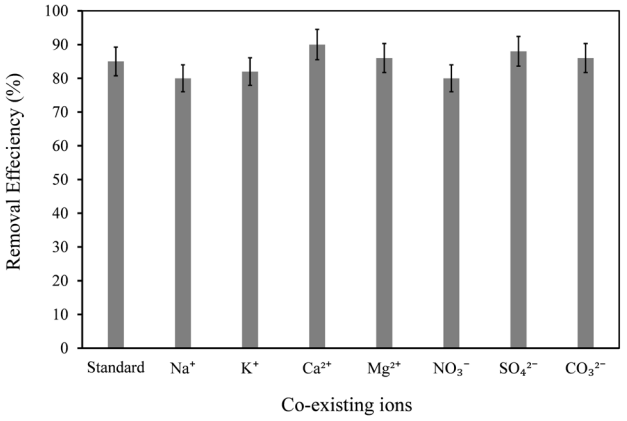

Fig. 7. Effect of co-existing ions on the removal efficiency of Cr(VI).

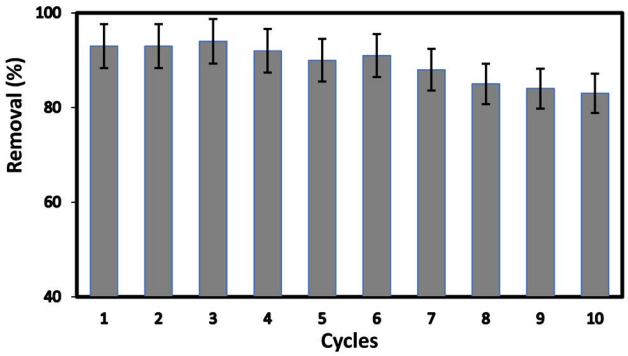

Fig. 8. The catalyst performance after 10 cycles of the regeneration process.

model was used for the evaluation of the impact of current density, initial concentration of Cr(VI), and time on the removal efficiency of the Cr(VI). A quadratic model was achieved, showing a noteworthy interaction between the initial concentration of Cr(VI), current density, and time. The results indicated that the Pd catalyst has a significant role in the removal process of Cr(VI). Under the optimal conditions and in the specified range of variables, the maximum removal efficiency of >98% was achieved. According to the results, at a higher current density, the prepared catalyst had a higher removal efficiency for the Cr(VI). Also, the results of the evaluation of catalyst recovery indicated that the performance of the prepared catalyst decreased about 10% after 10 cycles of usage.

Acknowledgments

The authors wish to thank the University of Kashan and the University of Tehran for their support.

References

[1] V.K. Gupta, I. Ali, Removal of lead and chromium from wastewater using bagasse fly ash – a sugar industry waste, J. Colloid Interface Sci., 271 (2004) 321–328.
[2] D. Mohan, S. Rajput, V.K. Singh, P.H. Steele, C.U. Pittman, Modeling and evaluation of chromium remediation from water using low cost bio-char, a green adsorbent, J. Hazard. Mater., 188 (2011) 319–333.
[3] R.A. Fallahzadeh, R. Khosravi, B. Dehdashti, E. Ghahramani, F. Omidi, A. Adli, M. Miri, Spatial distribution variation and probabilistic risk assessment of exposure to chromium in ground water supplies; a case study in the east of Iran, Food Chem. Toxicol., 115 (2018) 260–266.
[4] Y. Yao, J. Zhang, H. Chen, M. Yu, M. Gao, Y. Hu, S. Wang, Ni0 encapsulated in N-doped carbon nanotubes for catalytic reduction of highly toxic hexavalent chromium, Appl. Surf. Sci., 440 (2018) 421–431.
[5] H. Aslani, T. Ebrahimi Kosari, S. Naseri, R. Nabizadeh, M. Khazaei, Hexavalent chromium removal from aqueous solution using functionalized chitosan as a novel nano-adsorbent: modeling and optimization, kinetic, isotherm, and thermodynamic studies, and toxicity testing, Environ. Sci. Pollut. Res., 25 (2018) 20154–20168.
[6] W. Xu, H. Zhang, G. Li, Z. Wu, A urine/Cr(VI) fuel cell – electrical power from processing heavy metal and human urine, J. Electroanal. Chem., 764 (2016) 38–44.
[7] S. Mohan, G. Saravanan, N.G. Renganathan, Comparison of chromium coatings and electrochemical behaviour with direct current and pulse current deposition in trivalent chromium formate urea bath as alternative to conventional Cr coatings, Surf. Eng., 27 (2011) 775–783.
[8] Y. Zhang, M. Xu, H. Li, H. Ge, Z. Bian, The enhanced photoreduction of Cr(VI) to Cr(III) using carbon dots coupled TiO_2 mesocrystals, Appl. Catal., B, 226 (2018) 213–219.
[9] R. Jobby, P. Jha, A.K. Yadav, N. Desai, Biosorption and biotransformation of hexavalent chromium [Cr(VI)]: a comprehensive review, Chemosphere, 207 (2018) 255–266.
[10] J.H. Wu, F.Q. Shao, S.Y. Han, S. Bai, J.J. Feng, Z. Li, A.J. Wang, Shape-controlled synthesis of well-dispersed platinum nanocubes supported on graphitic carbon nitride as advanced visible-light-driven catalyst for efficient photoreduction of hexavalent chromium, J. Colloid Interface Sci., 535 (2019) 41–49.
[11] L.L. Wei, R. Gu, J.M. Lee, Highly efficient reduction of hexavalent chromium on amino-functionalized palladium nanowires, Appl. Catal., B, 176–177 (2015) 325–330.
[12] G. Qin, M.J. McGuire, N.K. Blute, C. Seidel, L. Fong, Hexavalent chromium removal by reduction with ferrous sulfate, coagulation, and filtration: a pilot-scale study, Environ. Sci. Technol., 39 (2005) 6321–6327.
[13] K. Liu, Z. Shi, S. Zhou, Reduction of hexavalent chromium using epigallocatechin gallate in aqueous solutions: kinetics and mechanism, RSC Adv., 6 (2016) 67196–67203.
[14] Y. Song, H. Dong, L. Yang, M. Yang, Y. Li, Z. Ling, J. Zhao, Hydrate-based heavy metal separation from aqueous solution, Sci. Rep., 6 (2016) 21389, doi: 10.1038/srep21389.
[15] J. Heffron, M. Marhefke, B.K. Mayer, Removal of trace metal contaminants from potable water by electrocoagulation, Sci. Rep., 6 (2016) 28478, doi: 10.1038/srep28478.
[16] Y. Ku, I.L. Jung, Photocatalytic reduction of Cr(VI) in aqueous solutions by UV irradiation with the presence of titanium dioxide, Water Res., 35 (2001) 135–142.
[17] X. Wang, S.O. Pehkonen, A.K. Ray, Removal of aqueous Cr(VI) by a combination of photocatalytic reduction and coprecipitation, Ind. Eng. Chem. Res., 43 (2004) 1665–1672.
[18] N.M. Dogan, C. Kantar, S. Gulcan, C.J. Dodge, B.C. Yilmaz, M.A. Mazmanci, Chromium(VI) bioremoval by *Pseudomonas* bacteria: role of microbial exudates for natural attenuation and biotreatment of Cr(VI) contamination, Environ. Sci. Technol., 45 (2011) 2278–2285.
[19] J. Regan, N. Dushaj, G. Stinchfield, Reducing hexavalent chromium to trivalent chromium with zero chemical footprint: borohydride exchange resin and a polymer-supported base, ACS Omega, 4 (2019) 11554–11557.
[20] S.A. Kazmi, M.U. Rahman, Kinetics and mechanism of conversion of carcinogen hexavalent Cr(VI) to Cr(III) by reduction with ascorbate, J. Chem. Soc. Pak., 19 (1997) 201–204.
[21] X.-R. Xu, H.-B. Li, X.-Y. Li, J.-D. Gu, Reduction of hexavalent chromium by ascorbic acid in aqueous solutions, Chemosphere, 57 (2004) 609–613.
[22] I.J. Buerge, S.J. Hug, Kinetics and pH dependence of chromium(VI) reduction by iron(II), Environ. Sci. Technol., 31 (1997) 1426–1432.
[23] V. Khain, V. Martynova, A.A. Volkov, Reduction of chromium(VI) to chromium(III) with sodium borohydride in an alkaline solution, Inorg. Mater. (English Transl.), 24 (1988) 376–379.
[24] P. Demirçivi, G. Saygılı, Removal of boron from waste waters by ion-exchange in a batch system, World Acad. Sci. Eng. Technol., 47 (2008) 95–98.
[25] F. Rodriguez-Valadez, C. Ortiz-Éxiga, J.G. Ibanez, A. Alatorre-Ordaz, S. Gutierrez-Granados, Electroreduction of Cr(VI) to Cr(III) on reticulated vitreous carbon electrodes in a parallel-plate reactor with recirculation, Environ. Sci. Technol., 39 (2005) 1875–1879.
[26] H. Zhang, W. Xu, Z. Wu, M. Zhou, T. Jin, Removal of Cr(VI) with cogeneration of electricity by an alkaline fuel cell reactor, J. Phys. Chem. C, 117 (2013) 14479–14484.
[27] E. Rahimi, G. Sajednia, M. Baghdadi, A. Karbassi, Catalytic chemical reduction of nitrate from simulated groundwater using hydrogen radical produced on the surface of palladium catalyst supported on the magnetic alumina nanoparticles, J. Environ. Chem. Eng., 6 (2018) 5249–5258.
[28] N. Mei, B. Liu, Pd nanoparticles supported on Fe_3O_4@C: an effective heterogeneous catalyst for the transfer hydrogenation of nitro compounds into amines, Int. J. Hydrogen Energy, 41 (2016) 17960–17966.
[29] S. Hokkanen, A. Bhatnagar, M. Sillanpää, A review on modification methods to cellulose-based adsorbents to improve adsorption capacity, Water Res., 91 (2016) 156–173.
[30] D. Wang, A critical review of cellulose-based nanomaterials for water purification in industrial processes, Cellulose, 26 (2019) 687–701.
[31] X. Chen, L. Liu, Z. Luo, J. Shen, Q. Ni, J. Yao, Facile preparation of a cellulose-based bioadsorbent modified by hPEI in heterogeneous system for high-efficiency removal of multiple types of dyes, React. Funct. Polym., 125 (2018) 77–83.
[32] R. Kumar, R.K. Sharma, Synthesis and characterization of cellulose based adsorbents for removal of Ni(II), Cu(II) and Pb(II) ions from aqueous solutions, React. Funct. Polym., 140 (2019) 82–92.

[33] R. Araga, C.S. Sharma, Amine functionalized electrospun cellulose nanofibers for fluoride adsorption from drinking water, J. Polym. Environ., 27 (2019) 816–826.
[34] G. Sajednia, E. Rahimi, N. Alvand, A. Karbassi, M. Baghdadi, Fibrous adsorbent derived from sulfonation of cotton waste: application for removal of cadmium sulfide nanoparticles from aquatic media, SN Appl. Sci., 1 (2019) 1525, doi: 10.1007/s42452-019-1525-x.
[35] L. Jin, L. Chai, L. Ren, Y. Jiang, W. Yang, S. Wang, Q. Liao, H. Wang, L. Zhang, Enhanced adsorption-coupled reduction of hexavalent chromium by 2D poly(m-phenylenediamine)-functionalized reduction graphene oxide, Environ. Sci. Pollut. Res., 26 (2019) 31099–31110.
[36] D. Rajalaxmi, N. Jiang, G. Leslie, A.J. Ragauskas, Synthesis of novel water-soluble sulfonated cellulose, Carbohydr. Res., 345 (2010) 284–290.
[37] E.H. Portella, D. Romanzini, C.C. Angrizani, S.C. Amico, A.J. Zattera, Influence of stacking sequence on the mechanical and dynamic mechanical properties of cotton/glass fiber reinforced polyester composites, Mater. Res., 19 (2016) 542–547.
[38] N. Tafreshi, S. Sharifnia, S.M. Dehaghi, Box–Behnken experimental design for optimization of ammonia photocatalytic degradation by ZnO/Oak charcoal composite, Process Saf. Environ. Prot., 106 (2017) 203–210.